**Department of Pesticide Regulation**
**Environmental Monitoring Branch**
**1001 I Street, P.O. Box 4015**
**Sacramento, CA 95812-4015**

# Modeling the high detections of 1,3-Dichloropropene in DPR's Air Monitoring Network

Yuzhou Luo, Ph.D., Research Scientist IV

Rosemary Uyeda, Environmental Scientists

4/3/2023

## 1 Introduction

1,3-Dichloropropene (1,3-D) is a fumigant used to control nematodes, insects, and disease organisms in the soil. It is commonly used as a pre-plant treatment that is injected into soil. It may also be applied through drip irrigation. The possibility of offsite transport of this fumigant due to volatilization may subsequently result in human exposure through inhalation. The Department of Pesticide Regulation (DPR) sets regulatory target concentrations for both cancer risk and acute exposure. To control lifetime cancer risk, DPR limits the use of 1,3-D to a 95% probability of achieving a regulatory target concentration of no more than 0.56 ppb as a 70-year average (Marks, 2016). To address acute exposures to bystanders from 1,3-D, DPR established a regulatory target concentration of 55 ppb averaged over a 72-hour period (DPR, 2021).

An air monitoring network (AMN) has been developed by DPR to assess the acute and chronic exposures from 1,3-D uses. In addition, an air dispersion model, AERMOD (American Meteorological Society/Environmental Protection Agency Regulatory Model), is currently used to predict ambient concentrations of soil fumigants including 1,3-D. This model has been validated for its modeling capability on regulatory modeling with long-term, regional simulations (Luo, 2019a). For site-specific modeling, however, results of previous modeling efforts warranted additional evaluation and development on AERMOD. As a Gaussian plume model, AERMOD is designed to provide the probability distribution of ambient concentrations of an air pollutant in response to given source emissions. It's not expected to exactly match air monitoring results at specific sampling sites and periods (USEPA, 2005). To better understand the relationship between the reported 1,3-D uses and observed concentrations, spatiotemporal variabilities are introduced in air dispersion modeling, so that the observations could be captured within the range of model predictions. Spatial modeling approach has been implemented to search the locations surrounding the monitoring site (Barry, 2015; Johnson, 2014; Luo, 2019a; van Wesenbeeck et al., 2013), representing the uncertainties on wind directions and source locations. In addition, the variability on soil properties and associated flux estimates were also considered. For example, the soil dataset with the highest emission fluxes was used in the modeling and expected to predict the upper bound of concentrations that could be measured at a monitoring site (Tao, 2018a, b, 2019).

To extend the previous modeling efforts, this study develops and tests a systematical modeling approach based on AERMOD to evaluate the high detections of 1,3-D observed in the AMN. This approach incorporates the uncertainty and variability of input parameters into the site-specific modeling, including the magnitudes and alignments of hourly 1,3-D emission fluxes and hourly meteorological data during a sampling period. The proposed modeling approach and computer tools are anticipated to help understand the effects of source emissions, soil properties, and meteorological conditions on the measured concentrations of 1,3-D.

## 2 Previous data analysis and modeling for ambient concentrations of 1,3-D

The relationship between the use data of pesticides and the measured ambient concentrations (i.e., the use-concentration relationship) has been explored by DPR with statistical and mathematical modeling approaches. A regression analysis was performed with the reported use data and AMN measurements of chloropicrin in Salinas during 2013 and 2014 (Brown, 2015). A moderate correlation was confirmed between applied masses (within an initial search radius of 4 miles) and ambient concentrations. It's observed that applications far away from the monitoring site could also influence the AMN detections. For example, the potential sources for a single quantifiable detection in 2013 could not be located until increasing the search radius to 7 miles. Once the primary sources had been identified, however, further increasing the search radius did not improve the general performance of regression analysis.

Similar data analysis was conducted for 1,3-D (Brown, 2016), methyl bromide (Craig and Budahn, 2016), chlorpyrifos and chlorpyrifos-oxon (Budahn, 2016), chlorthal-dimethyl (King, 2016), and methyl isothiocyanate (Collins, 2016). In the study for 1,3-D, a regression equation was established between the 24-hour concentration measurements (log-transformed, at Shafter and Ripon sites during 2013–2014) and daily 1,3-D use (in adjusted total pounds or ATP) during the lag periods of 0 and 7 days before the end of sampling and within a 5-mile radius. Most of the data points illustrated a moderate positive correlation between the concentrations and uses. However, a significant portion of positive detections remained unassociated with any application records in the search domain (5 miles and 7 days prior to the completion of each air sample). Results of the study suggested further investigations on PUR reporting errors, source emissions, and meteorological data especially wind (Brown, 2016).

In order to estimate the township cap for 1,3-D, Tao (2016) paired annual average concentrations of 1,3-D measured in 9 communities with 1,3-D annual uses (in ATP) in a township-size area ($6\times6$ mi$^2$) around the sampling sites during 2006 to 2015. The linear relationships were not statistically confirmed between the annual average concentrations and annual uses. Therefore, only the ratios of concentration/use were calculated to determine the township caps of 1,3-D.

Early efforts of air dispersion modeling on monitoring data of 1,3-D were focused on the measurements by DAS (Dow AgroSciences) at 9 sites in Merced County. The DAS monitoring was conducted with continuous 72-hr sampling periods over 14.5 months mainly in 2011 (Rotondaro and van Wesenbeeck, 2012). Based on the ISCST3 (Industrial Source Complex – Short Term, version 3), the average concentrations were underpredicted at some monitoring sites, mainly related to the underestimation of the high detections in December 2011 (van Wesenbeeck et al., 2013). Therefore, a spatial modeling approach, with a receptor grid of

approximately 580m × 580m, was used to determine whether the model was predicting those high detections at locations surrounding the exact locations of monitoring sites. The modeling results indicated that the model predictions recovered the observed concentrations, but not necessarily at the precise locations where these high detections occurred. Similar modeling approach was used by DPR in the evaluation of AERMOD for simulating the Merced County monitoring data (Luo, 2019a). The study concluded that, although the model may significantly underestimate at some site locations, it could predict comparable value of annual average concentrations within a short distance from the corresponding sites.

A series of AERMOD modeling studies were conducted to predict relatively high concentrations of 1,3-D observed in the AMN, including (1) 15.96 ppb at Parlier, sampling started on 9/19/2017 (Tao, 2018b), (2) 50.5 ppb at Shafter, 1/22/2018 (Tao, 2018a), and (3) 110 ppb at Parlier, 10/9/2018 (Tao, 2019). Model simulations were based on the 1,3-D uses report in the surrounding fields (within about 1 mi), HYDRUS-generated flux profiles, and nearby NWS and CIMIS weather stations. The maximum predictions (modeled with the flux profiles for soil #5) were compared to the monitoring data (Figure 1). Predicted concentrations were comparable to the high detection at Shafter, but significantly underestimated the other two at Parlier with P/O ratios (i.e., prediction concentration divided by observed concentration) of 2.4% (for the sampling started on 9/19/2017) and 32% (10/9/2018).

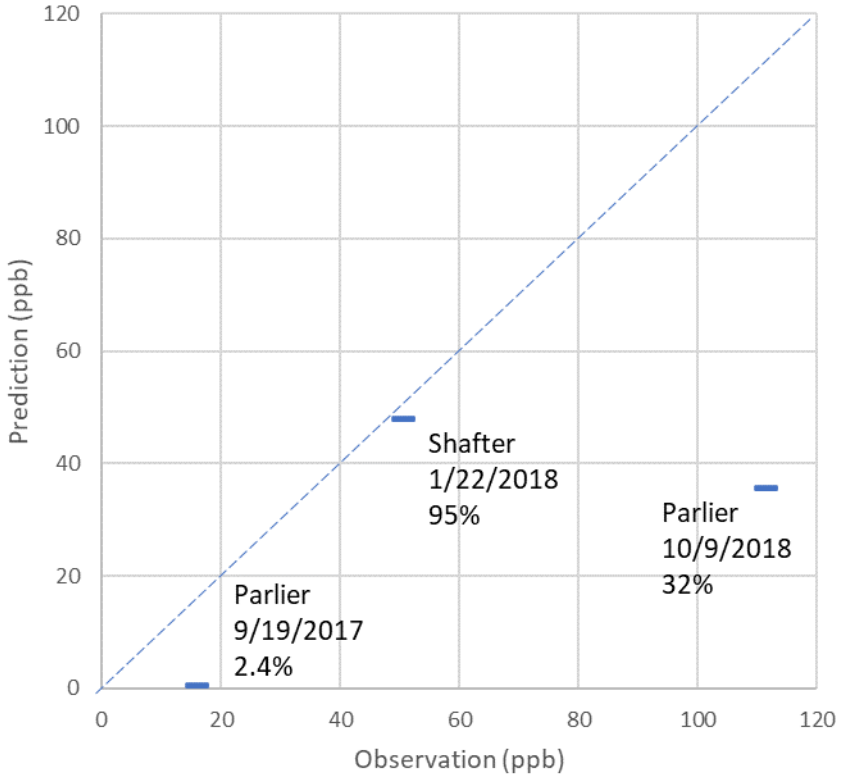


Figure 1. Previous modeling results 3 high detections in the AMN (Tao, 2018a, b, 2019), showing the maximum predictions modeled with the flux profiles for soil #5

## 3 Ambient air monitoring and high detections of 1,3-D

In 2006, DPR and California Air Resources Board (CARB) conducted air monitoring for 1,3-D ambient concentrations in Parlier, Fresno County (Segawa et al., 2006). In 2011, DPR established an air monitoring network (AMN) to sample ambient air for pesticides including 1,3-D in multiple communities on a regular schedule. The AMN collected a 24-hour sample each week to measure airborne concentration of 1,3-D. The monitoring data are used to evaluate and improve protective measures against pesticide exposure. For example, according to the risk management directive for 1,3-D (Marks, 2016), DPR requires additional evaluations if air monitoring shows one-year average air concentrations above 0.27 ppb.

This study uses the monitoring database revision 12142022 (December 14, 2022) posted online (www.cdpr.ca.gov/docs/emon/airinit/pesticide_air_monitoring_database.htm). In the database, there are 4,313 records of 1,3-D reported at 19 site locations during 2010 to 2022. The overall detection frequencies of 1,3-D for all sites ranged from 19% to 57% in the recent 5 years (Table 1). Higher frequencies were observed at the sites of Parlier and Shafter. Note that the monitoring results include samples from both DPR and ARB. The method detection levels (MDLs) are 0.01 ppb for DPR measurements and 0.1 ppb for ARB. For more meaningful comparison, therefore, the detection frequencies are highlighted in Table 1 if the corresponding monitoring results were dominated by DPR samples (>50%).

Table 1. Detection frequency of 1,3-D in the air monitoring network. Highlighted value indicates a site-year with >50% DPR samples (MDL=0.01 ppb)

| | 2017 | 2018 | 2019 | 2020 | 2021 |
|---|---|---|---|---|---|
| All sites | 26% | 25% | 19% | **57%** | **55%** |
| Parlier | **67%** | **84%** | **83%** | **78%** | **75%** |
| Shafter | **48%** | 38% | 10% | **70%** | **69%** |

In this study, a "high detection" of 1,3-D is defined as a measured concentration larger than 10 ppb over a 24-h sampling period. The cutoff value of 10 ppb represents extremely high values of 1,3-D measurements in the AMN (> the 99$^{th}$ percentile). Based on the weekly sampling interval, a single high detection above 10 ppb would contribute more than 70% of the one-year target concentration of 0.27ppb (10/52/0.27=71%) as the DPR's criterion for additional evaluation. Two high detections in a year will result in a one-year average concentration exceeding 0.27 ppb, as observed in 2020 at Shafter and 2021 at Parlier.

Based on the cutoff value of 10 ppb, in total 8 measurements of 1,3-D in the AMN are identified as high detections for further investigation in this study (Table 2). All high detections were reported at the sites of Parlier and Shafter. The highest concentration of 111.29 ppb was measured at Parlier during a 24-hr sampling period on October 9~10, 2018 ([2] in Table 2). The Parlier sampling site is located at the University of California's Kearney Agricultural Research and Extension Center (-119.503705, 36.597491). In February 2019, the Shafter site was relocated from Shafter High School (-119.265733, 35.508822) to Sequoia Elementary (-119.268763, 35.516477). The heights of samplers are 4 m at the Parlier site, 3 m at the old Shafter site, and 3.2 m at the new Shafter site.

Table 2. High detections of 1,3-D reported in the AMN during 2010-2022

| ID | Site | Start date | Start time | Conc (μg/m$^3$) | Conc (ppb) |
|---|---|---|---|---|---|
| [1] | Parlier | 09/19/2017 | 15:43 | 72.44 | 15.96 |
| [2] | Parlier | 10/09/2018 | 16:37 | 505.11 | 111.29 |
| [3] | Parlier | 10/16/2020 | 07:00 | 48.16 | 10.61 |
| [4] | Parlier | 02/22/2021 | 16:00 | 63.54 | 14.00 |
| [5] | Parlier | 09/08/2021 | 11:00 | 113.15 | 24.93 |
| [6] | Shafter | 01/22/2018 | 12:00 | 229.16 | 50.49 |
| [7] | Shafter | 01/12/2020 | 13:08 | 94.40 | 20.80 |
| [8] | Shafter | 10/16/2020 | 13:29 | 170.20 | 37.50 |

# 4 Model development and simulation design

## 4.1 Overview of modeling approaches

Model simulations in this study are managed by AERFUM, an integrated air dispersion modeling system for soil fumigants developed by DPR (Luo, 2019b). AERFUM employs AERMOD version 22112 as the core simulation engine for air dispersion modeling and provides pre- and post-processing functions specifically designed for fumigations at various spatiotemporal scales. AERFUM is optimized for model applications in California by incorporating pesticide use data, meteorological data, and geographic information system (GIS) layers. AERFUM has been validated with measured 1,3-D concentrations in California as annual averages and 95$^{th}$ percentiles (Luo, 2019a), and the predictions in most of the years and sites were within the factor of 2 of the measured values. The results support the use of AERMOD for regulatory modeling on soil fumigants with regional and long-term simulation of ambient air concentrations. The model is being used to determine the application factors, township caps, and setback distances of 1,3-D.

On-site meteorological data are retrieved from DPR's weather stations collocated at the AMN sites and supplemented by the data from ARB's Air Quality and Meteorological Information System (AQMIS, www.arb.ca.gov/aqmis2/aqmis2.php). Additional surface and upper air data are taken from the NOAA's National Weather Service (NWS). The AQMIS station at Parlier is collocated with DPR's monitoring site, and the "Shafter-Walker Street" station is about 0.5 and 1 mi to the previous (before 2019) and new locations of Shafter monitoring site, respectively. The MetProc program is used to prepare input meteorological data for air dispersion modeling (Luo, 2017).

Table 3. Meteorological data sources used in this study

| AMN site | Parlier | Shafter |
|---|---|---|
| NWS station | 93193 (Fresno Yosemite International Airport) | 23155 (Meadows Field Airport) |
| AQMIS station | 2114 (Parlier) | 2981 (Shafter-Walker Street) |
| DPR station | Parlier (2019 and after) | Shafter (2019 and after) |
| Upper air station | OAK (Oakland International Airport) | VBG (Vandenberg AFB) |

A two-step modeling procedure is implemented in this study for evaluating 1,3-D high detections, including (1) standard "regional simulation" by considering the variability on soil

properties and associated emission fluxes, and (2) additional modeling by incorporating variability and uncertainty on hourly flux data and wind data. Note that the step (2) is only needed when (1) is not able to capture the observations.

## 4.2 Standard regional simulations with various soil datasets and associated flux profiles

Two types of simulations are implemented in AERFUM (Luo, 2019b): (1) Unit simulation, which evaluates a single application event for the potential air concentrations at field scale; and (2) Regional simulation, which continuously simulates reported pesticide uses at sub-regional scale, and the results could be compared to measured concentrations from air monitoring networks. A 3×3 township area (about 18 × 18 $mi^2$) is commonly used as modeling area in the AERFUM regional simulation, with the receptors of interest located in the center township (Figure 2). This configuration was taken from DPR's previous modeling studies on chronic risk from 1,3-D (Barry and Kwok, 2016; CDPR, 2015; Johnson, 2007a, b), and recently used in the model validation with the long-term statistics of monitoring data (Luo, 2019a).

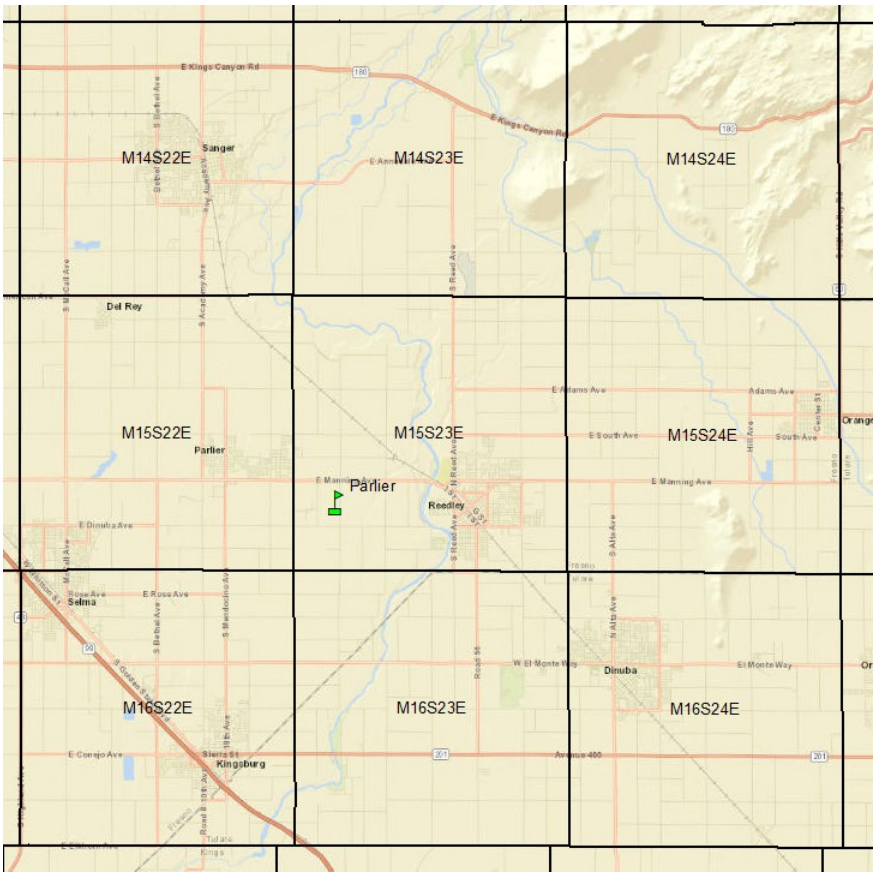


Figure 2. The simulation domain as 3×3 township area, for the monitoring site at Parlier as an example.

In this study, the regional simulation of AERFUM predicts the concentration of 1,3-D averaged over the sampling period at the monitoring site (Table 2) based on the reported pesticide use data in the simulation domain. Specifically, the simulation domain is defined as,

*Time*: the antecedent applications of 1,3-D reported within a 10-d timespan prior to the end of sampling. For example, if a high detection to be modeled was sampled during 9/19/2017 to 9/20/2017, reported applications on and after 9/10/2017 will be modeled.

*Space*: 1,3-D applications reported within the 3×3 township area (with the site located in the center township): M14S21E, M14S22E, M14S23E, M15S21E, M15S22E, M15S23E, M16S21E, M16S22E, M16S23E for Parlier (Figure 2), and M27S24E, M27S25E, M27S26E, M28S24E, M28S25E, M28S26E, M29S24E, M29S25E, M29S26E for Shafter.

This study demonstrates the modeling within a 3×3 township area. This represents the general option to define a modeling area with user-specified townships, e.g., a 5×5 township area or a list of any townships are also acceptable (Luo, 2022). In addition, AERFUM provides other options to define a modeling area (Luo, 2019b). The following two options could be useful for the high-detection modeling: (1) user-specified sections, or (2) user-specific centroid and radius with which AERFUM will automatically retrieve sections.

Within each simulation domain, application data of 1,3-D are retrieved from DPR's pesticide use report (PUR) database for the years of 2017-2021. Note that, as of this study, PUR data for 2021 are still under review by DPR and not publicly released in the California Pesticide Information Portal (CalPIP). For each 1,3-D application, the extracted data as model inputs include the treated acreage, rate, date, time and fumigation method. Application events are reported at the spatial resolution of section (1×1 $mi^2$) following the U.S. Public Land Survey System (PLSS), but the exact location and dimensions of a treated field are not specified in PUR. In the previous version of AERFUM, each treated field (i.e., a source) is modeled as a square, and randomly located within the reported section (Luo, 2019b). In this study, AERFUM is improved with refined source placement by incorporating the GIS data of field boundaries in the Cal Ag Permits (CAP) system. CAP data specify the location and dimension of each treated field. Specifically, the section ID, field ID, and permit number of an application from the PUR database are matched with those in the CAP data of field boundaries in order to determine the location and dimensions of each treated field for air dispersion modeling. This new function in AERFUM improves the spatial resolution of source characterization from section to field scale.

During the study period of 2017-2021, there were 17 field fumigation methods (FFM) actively recognized in California (Appendix I). Hourly emission fluxes (called "flux profiles" thereafter) of 1,3-D are generated by HYDRUS modeling. Two sets of flux profiles, generated in 2019 (Brown, 2019) and 2022 (Brown, 2022), are used in this study and referred as the 2019 profiles and 2022 profiles, respectively. Normalized by a reference application rate of 100 lb/ac, each flux profile consists of hourly emission rates ($\mu g/m^2/s$) of 1,3-D for a total duration of 500 hours after the completion of application. For each application method of 1,3-D, profiles are modeled with multiple soil datasets sampled in previous fumigant field studies, representing the variabilities in soil properties especially soil water content. The 2019 flux profiles include 16 soils, while the 2022 profiles modeled 21 soils including all soils in the 2019 study and 5 new soils recently sampled. For the same FFM, the predicted flux data, in terms of the maximum 24-h flux or other statistics, are negatively correlated with the soil water content as a percentage of field capacity (pFC) (Kandelous and Brown, 2019). For example, soil #5 is measured with the

lowest pFC (25%) and predicted with the highest flux over all modeled soils in both sets of flux profiles.

For the same soil, the differences of predicted flux values between the two studies are mainly attributed to the estimation on soil organic carbon (OC) content (Brown, 2022). The OC contents are not measured for most of the soils especially in the original 16 soils. Therefore, the OC contents were estimated for the soils without field measurements. Compared to the 2019 profiles, the 2022 ones are generally associated with higher OC estimates, resulting in lower emissions. Taking the soil #5 and FFM1206 ("Nontarpaulin/Deep/Broadcast or Bed") as an example, the maximum 24-hour flux is 18.09 $\mu g/m^2/s$ in the 2022 flux profiles, 44% lower than that in the 2019 flux profiles (32.59 $\mu g/m^2/s$). In summary, the two sets of 1,3-D flux profiles are used in this study to represent the variability and uncertainty on soil water content and OC content. This study will run air dispersion modeling with all available flux data (16 soils in the 2019 profiles and 21 soils in the 2022 profiles), and report the minimum, maximum, and average predictions.

### 4.3 Evaluations with additional variabilities and uncertainties

A successful site-specific modeling on high detections requires accurate input data for each hour of the sampling period at the sampling location. The standard regional simulations assume that the hourly inputs of pesticide applications, emission fluxes, and meteorological data accurately reflect the field conditions during the sampling periods. However, the input data may not sufficiently represent the site-specific conditions. Results of the preliminary uncertain analysis in the previous studies recommended further assessment on the flux profiles and wind directions. In this study, the effects of the uncertainties in flux profiles and wind data on 1,3-D high detection modeling are mathematically represented by shifting the following input parameters around their reported values. The justification and implementation are provided in the next paragraphs.

[1] The start hour of a flux profile = reported application time ± 12 hours (or a user-specified value, in 1-hour increments). This study uses ±12 hours for demonstration (Figure 3), and in total 25 instances (including the original one with dt = 0) will be generated for each flux profile.
[2] For each hour during the sampling period, the wind direction is randomized within a range of plume centerline directions determined from the standard deviation of lateral wind direction in the corresponding hour.

*Temporal shifting of flux profiles*

The purpose of shifting the flux profile is to reflect the uncertainties on (1) the predicted timing of peak emission rates after application, (2) the prescribed completion time of 1,3-D application in the modeling of all flux profiles, and (3) the reported application date and time in PUR. The currently used flux profiles for 1,3-D are generated by HYDRUS with soil properties sampled in field studies, and meteorological data summarized from the month of Septembers between 2012-2016 from the CIMIS station #2 at Five Points, Fresno County. When applied to statewide field conditions, the flux profiles for each application method are assumed to represent the range of soil and meteorological conditions for the emission of fumigants at least for the high-use areas.

This assumption is more appropriate for regulatory modeling studies at large spatial scale and/or longer simulation periods.

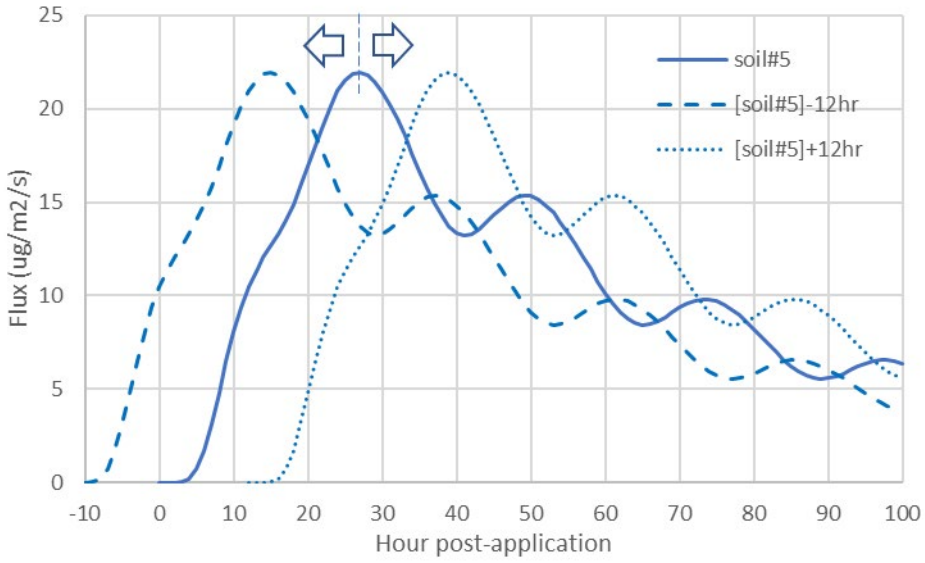


Figure 3. Demonstration of the times of peak emission rates in flux profiles and their shifting for uncertainty analysis, showing the 2022 flux profiles of FFM 1206 for soil #5 as an example

For site-specific modeling on high detections, however, the prescribed soil types and meteorological data may not represent the actual conditions of the treated fields on the sampling periods for the high detections. Results of previous study suggested that emission rates are very sensitive to the water content and organic carbon content of soil. Those soil properties are associated with great uncertainty and variability over time and space. In addition, modeling for the relatively short-time period (24 hours) of monitoring data asks for accurate estimates of emission data at each hourly simulation time step. Currently, the HYDRUS-generated flux profiles are mainly validated by the maximum emission rate and total emission, while the hourly variation especially the timing of the peak fluxes is not sufficiently evaluated. Taking the FFM1206 as an example, the HYDRUS-predicted times of the maximum emission rates ranged from 20 to 30 hours after applications over the modeled soils, with a standard deviation of 26 hours. For sandy loam soil, field experiments by Dow AgroSciences reported the emission peak time at hour 70 in a 1991 study and hour 110 in a 2020 study (Ajwa, 2021). Although the timing of the maximum flux (or the maximum period-average flux) does not significantly affect the results for regional, long-term modeling, it is critical to the modeling performance to replicate a high detection sampled within 24 hours.

In addition, the reported date and time for 1,3-D applications in the PUR database are associated with error and uncertainty (Wilhoit et al., 2001). It's not clear whether it is the time of start or completion of the applications, or just a representative time for applications. For example, applicators may lump multiple applications into a single event for reporting (Brown, 2016). Furthermore, the flux profiles were generated by assuming an instantaneous application of 1,3-D at 8AM. For comparison, flux profiles for selected application methods were also modeled at 12PM and 4PM (Colin Brown, 2019, unpublished data), which have higher and sooner peak

emission rates compared to that at 8AM. For soil #5 as an example, the predicted peak flux rates are 40.0 (at hour 26), 45.6 (hour 22), and 48.8 (hour 19) μg/m$^2$/s, for the completion time at 8AM, 12PM, and 4PM, respectively. In summary, the temporal shifting of the flux profiles is used in the 1,3-D high detection modeling to represent all above-discussed variabilities and uncertainties on the hourly flux data in the profiles.

*Spatial shifting of wind directions*

The purpose of spatial shifting is to reflect the uncertainties on (1) the wind directions modeled at the site location and height and (2) the aggregation of sub-hourly wind direction measurements to hourly data for use in modeling. Four weather data sources have been used for wind data in this study (Table 3) and previous studies (Tao, 2018a, b, 2019) to model the high detections of 1,3-D at Parlier: NWS, CIMIS, AQMIS, and DPR (2019 and after). The standard deviations of wind direction among the meteorological datasets ranged from 0~103 degrees during 2017-2021 with an average of 23 degrees. Even at the same station, differences of wind directions measured at different heights are observed. For example, DPR measured wind data at Parlier with sensor heights of 2 m and 10 m. The measured wind directions in 2020 were statistically different based on the paired t test ($p < 0.001$) and the mean difference is about 4 degrees per minute. At the same height of the same station, in addition, the aggregation of sub-hourly wind data into hourly data could propagate uncertainty into air dispersion modeling. According to the reported data at the nearby CIMIS station, the standard deviations of wind direction for each hourly record at Parlier were measured from 0~84 degrees during 2017-2021, with an average of 33 degrees. That means the measured sub-hourly wind directions could be significantly different from the hourly averages used in air dispersion modeling.

The standard deviation of the lateral wind direction ($\sigma_\theta$) is first calculated from the onsite sub-hourly meteorological data based on the Yamartino (1984) method. If the onsite data are not available or not sufficient for the calculation, the $\sigma_\theta$ values could be retrieved from the nearby CIMIS station. For the sampling periods modeled in this study, the 24-hour average $\sigma_\theta$ is about 40 degree and associated with great variations from hour to hour.

The $\sigma_\theta$ value is used to estimate the bounds on the plume centerline direction (Sajo, 2003). The spatial uncertainty is estimated as the half width of the confidence interval on the plume centerline ($\Delta\vartheta$),

$$\Delta\vartheta = \tan^{-1}(\sigma_\theta \sqrt{G(n,\sigma_l)})$$

where $G(n,\sigma_l)$ is a scaling parameter as a function of $n$ (factor of validity) and $\sigma_l$ (logarithmic standard deviation of the local concentration),

$$G(n,\sigma_l) = -\sigma_\theta \pm \sqrt{4\ln^2(n) + 12\sigma_l{}^2 \ln(n) + \sigma_l{}^4}$$

For ground level sources under low wind speed conditions, the reported predicted-to-observed concentration ratios ranged from 1 to 100 with a representing $\sigma_l$ of 1.77 (Miller and Hively, 1987). With a commonly used confidence interval of 95%, the $n$ value is estimated as 6 based on

Eq. (A5) by Sajo (2003). Therefore, the scaling parameter G(6, 1.77) = 6.35, and the half width of the confidence interval on plume centerline can be simplified as,

$$\Delta\vartheta = \tan^{-1}(2.52\sigma_\theta)$$

In an hour with $\sigma_\theta$= 0.70 rad (40 deg), for example, $\Delta\vartheta$ is calculated as 60.4 deg, i.e., there is 95% confidence that the plume centerline is within ±60.4 deg of the modeled direction. A similar approach has been used in the previous DPR study for modeling a high detection of methyl isothiocyanate (Barry, 2005).

For computer implementation in this study, the $\Delta\vartheta$ value is first calculated for each hour during the sampling period. Monte Carlo simulations are conducted by altering the wind direction with a random incremental azimuthal angle within $\pm\Delta\vartheta$ for the corresponding hour. Random sampling is independent from hour to hour (in contrast to applying one value to all hours in each model run). Results of 1,000 model runs are reported in this study (Section 5.3).

# 5 Results

## 5.1 Standard regional simulations

Modeling results from the standard regional simulation of AERFUM vary greatly with the input flux profiles (Figure 4). For most of high detections modeled in this study, the maximum predictions are associated with the flux profiles for soil #5. The only exception is for the high detection [6] (50.49 ppb, Shafter, 1/22/2018), for which the maximum prediction with soil #9 is slightly higher than that with #5.

Compared to other soils, the flux profiles for soil #5 have the highest rates in terms of the max 24-h flux, 72-h flux and emission ratio. In addition, the relative timing between applications and sampling also affect the model predictions. For the 2019 profiles on FFM1206 as an example, although soil #9 are associated lower peak and total emissions compared to soil #5, some of the hourly flux rates of soil #9 are higher than soil #5, such as hours 30 to 36 and 51 to 63. This explains the maximum prediction with the flux profiles for soil#9 for the high detection [3]. More details are provided in the later sections 5.3 (for the primary sources) and 6 (for the relative timing between applications and sampling).

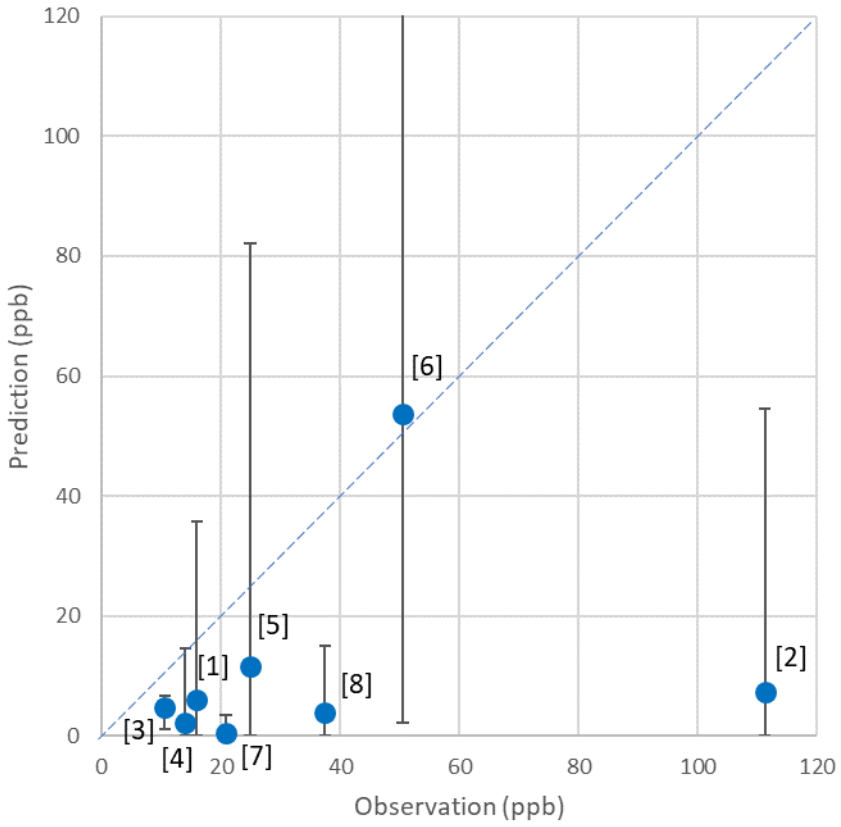


Figure 4. Results of AERFUM regional simulations, showing the minimum, average (blue circles), and maximum predictions over the 37 flux profiles. See Table 2 for the ID of the modeled high detections

Figure 5 shows an example of model predictions varying with the flux profiles representing various soil water content as percent of field capacity (pFC). There is a general decreasing trend of predicted concentrations with the increase of pFC. In addition to soil water content, the soil OC content is also an important influencing factor. With lower estimates of OC, the 2019 flux profiles predict higher concentrations than the 2022 profiles for most of the soils (Figure 5).

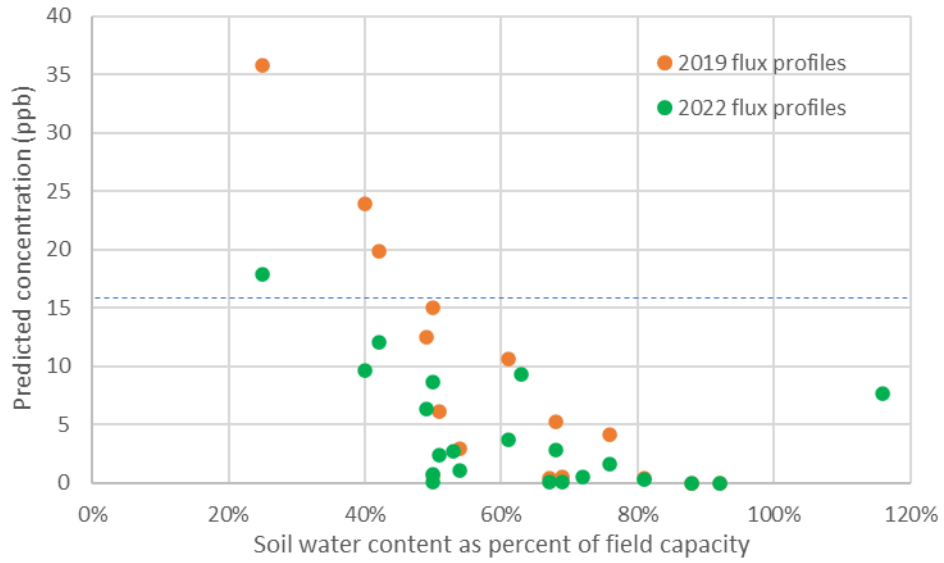


Figure 5. Model predictions varying with the soil properties in the flux profiles, showing the results for the high detection [1] (the dashed line of 15.96 ppb, Parlier, 9/19/2017)

The modeling performance is evaluated by comparing each high detection to the range of predictions. A satisfactory modeling is defined if the measured concentration is within the range, i.e., the observation is well captured by the model simulations with various flux profiles. Otherwise, the model underestimates the high detection if even the highest prediction is below the measured concentration. In this case, the modeling performance is characterized by a P/O ratio, i.e., the ratio between the maximum prediction and the observed concentration. Theoretically, there is the third situation where the lowest prediction is above the measured concentration, but this has not been observed in this and previous studies for 1,3-D high detections.

By comparing the range of predicted concentrations with the measurements (Table 4), the regional simulations of AERFUM well predict 4 high detections: [1] (15.96 ppb, Parlier, 9/19/2017), [4] (14 ppb, Parlier, 2/22/2021), [5] (24.93 ppb, Parlier, 9/8/2021), and [6] (50.49ppb, Shafter, 1/22/2018). For the highest detection [2] (111.29 ppb, Parlier, 10/9/2018), the maximum prediction (54.6 ppb) is only about half of the measured value (P/O ratio = 49%). For the 3 high detections in 2020 ([3], [7], and [8]), the model also underestimated the observations with P/O ratios between 17% to 63%.

Table 4. Modeling results based on standard regional simulations

| ID | Site | Start date | Measured conc. (ppb) | Model performance (this study) | Model performance (previous studies, Figure 1) |
|---|---|---|---|---|---|
| [1] | Parlier | 09/19/2017 | 15.96 | S | 2.4% |
| [2] | Parlier | 10/09/2018 | 111.29 | 49% | 32% |
| [3] | Parlier | 10/16/2020 | 10.61 | 63% | - |
| [4] | Parlier | 02/22/2021 | 14.00 | S | - |
| [5] | Parlier | 09/08/2021 | 24.93 | S | - |
| [6] | Shafter | 01/22/2018 | 50.49 | S | 95% |
| [7] | Shafter | 01/12/2020 | 20.80 | 17% | - |
| [8] | Shafter | 10/16/2020 | 37.50 | 40% | - |

Notes: "S" for satisfactory modeling (i.e., the measurement is captured by the predicted range). Otherwise, a P/O ratio is reported for underestimation. See Figure 1 for more information on the previous studies.

Compared to the previous modeling efforts on the high detections [1], [2], and [6] (Tao, 2018a, b, 2019), the modeling performance in this study is generally improved. First, the regional simulations of AERFUM have a larger search domain for PUR data compared to the previous studies which only considered 1,3-D applications within a short distance (about 1 mi) from the monitoring site. Although the applications near to the monitoring sites are usually the primary sources to the high detections, other sources would also contribute to the measured concentrations.

The other improvement in this study is to use onsite meteorological data. Compared to the CIMIS data and NWS data used in the previous study, the onsite data better represent the meteorological conditions around the monitoring site. With a relative short modeling period of 24 hours, the predicted concentration values are extremely sensitive to meteorological data at each hour. For the high detection [1] as an example (Figure 6), during the sampling period started on 9/19/2017 in Parlier, the wind directions were generally from northwest in both NWS and CIMIS data, so the predicted concentrations were almost zero (0.34 ppb as 24-hr average with the flux profile of soil #5) for most hours since the monitoring site was located at upwind direction of the source (Tao, 2018b). However, the onsite AQMIS data used in this study captured a small number of hours with wind direction from southeast (Figure 6), resulting in high concentration predictions during those hours. As 24-hr averages, the predictions with AQMIS data in this study range from 6.1 to 35.8 ppb (Figure 4) which well bracket the observation of 15.96 ppb.

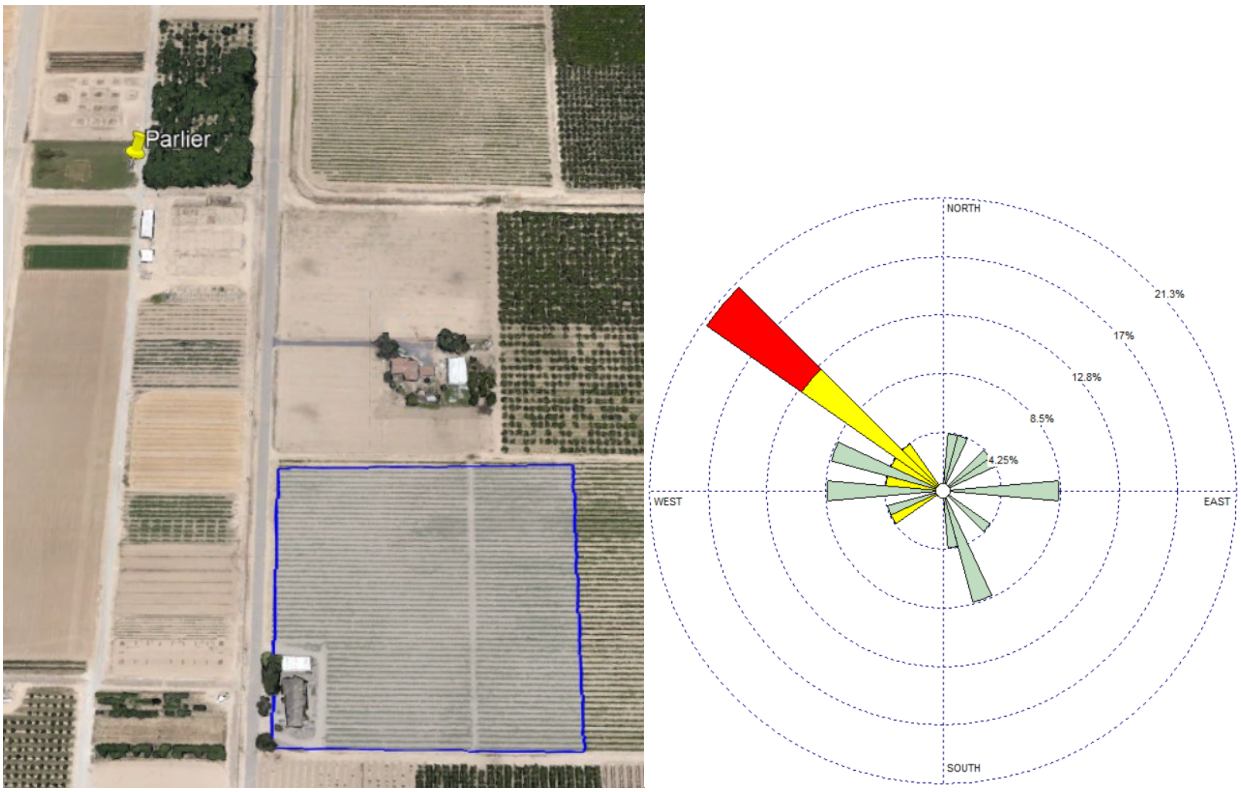


Figure 6. (Left) the locations of the monitoring site and treated field and (right) wind rose over the sampling hours for the high detection [1] (15.96 ppb, Parlier, 9/19/2017)

## 5.2 Application data and primary sources

Application data of 1,3-D modeled in this study are extracted from PUR for the simulation domain within a 3×3 township area and 10 days before the end of sampling (Table 5). The number of modeled 1,3-D applications ranged from 1 to 29. Most of the applications were reported with FFM 1206 ("Nontarpaulin/Deep/Broadcast or Bed") and FFM 1210 ("Nontarpaulin/Deep/Strip"). Only 4 out of the 88 modeled applications were associated with other methods of 1209 ("Tarpaulin/Chemigation/Bed") or 1247 ("TIF/Deep/Broadcast").

Table 5. 1,3-D application data and the primary sources modeled in this study

| ID | Site | Sampling start date | All sources | | Primary sources | | |
|---|---|---|---|---|---|---|---|
| | | | Number of applications | Total lbs. applied | Number of applications | Total lbs applied | Contribution to the predicted concentration |
| [1] | Parlier | 9/19/2017 | 3 | 4116 | 1 | 2923 | 100% |
| [2] | Parlier | 10/09/2018 | 25 | 48,856 | 4 (1) | 3305 | 97% |
| [3] | Parlier | 10/16/2020 | 12 | 48,411 | 1 | 9880 | 91% |
| [4] | Parlier | 02/22/2021 | 29 | 64,547 | 1 | 624 | 98% |
| [5] | Parlier | 09/08/2021 | 4 | 14,754 | 1 | 7270 | 100% |
| [6] | Shafter | 1/22/2018 | 7 | 48,864 | 1 | 7431 | 98% |
| [7] | Shafter | 1/12/2020 | 1 | 12,972 | 1 | 12,972 | 100% |
| [8] | Shafter | 10/16/2020 | 7 | 24,177 | 2 (2) | 6230 | 100% |

Notes: (1) in two groups: 2 adjacent fields (0.1 mi to the monitoring site, contributing 73% of the predicted total concentration, 24%) and another 2 adjacent fields (0.6 mi). (2) applications reported on consecutive days in 2 fields adjacent to each other.

To better investigate the use-exposure relationship for air dispersion modeling of 1,3-D, the primary sources are identified for each high detection (Table 5). The primary sources are defined based on their contributions to the total predicted concentration. The applications on adjacent fields may have similar concentrations and they are considered as a group of primary sources. For example, the model prediction for the high detection [2] (111.29 ppb, Parlier, 10/9/2018) was mainly contributed by 4 applications in two groups of adjacent applications. The identified primary sources account for 1~71% of the total modeled 1,3-D uses (except for the high detection [7] for which only 1 application is reported in the simulation domain) but contribute more than 90% of the predicted concentrations (Table 5).

Figure 7 shows the estimated distances between the primary sources and the corresponding monitoring sites. Five of the 8 high detections are related to primary sources within or close to 1 mi. The other 3 high detections ([3], [7], and [8]) are associated with primary sources relatively far away (2.7~8.2 mi) from the monitoring sites; those 3 measurements are all underestimated by the regional simulations (Table 4).

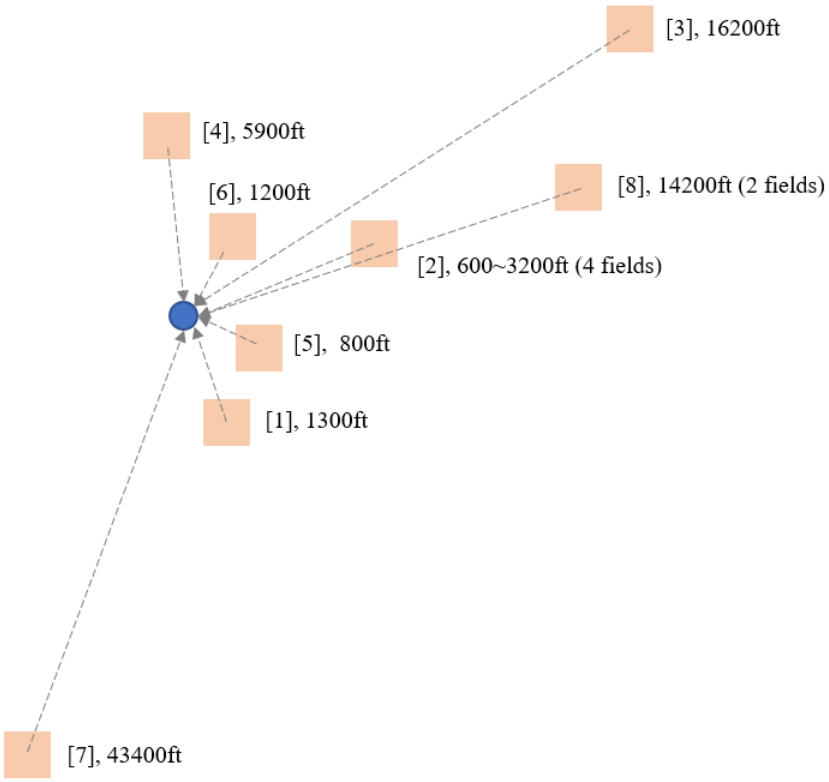


Figure 7. Schematic diagram for the relative locations of the monitoring sites (circle) and identified primary sources (square) for each high detection of 1,3-D. The locations, distances, sizes, and geometries in the diagram are not to scale but for illustration purpose only.

Temporally, except for the high detection [3] (10.61 ppb, Parlier, 10/16/2020), all primary sources were reported with 1,3-D applications within 24 hours of the start of sampling. For the high detection [3], the primary source of 1,3-D was applied 68 hours before the sampling, and this measurement is underestimated by the regional simulations of AERFUM (Table 4). All primary sources were associated with the FFMs of 1206 or 1210. For the two methods, the flux profiles suggested peak emission fluxes occurring in about 20~30 hours after application in both sets of flux profiles (Brown, 2019, 2022). The relative timing between the 1,3-D applications of the primary sources and the sampling period has significant effects on the model prediction of 24-hr average concentrations (Figure 8).

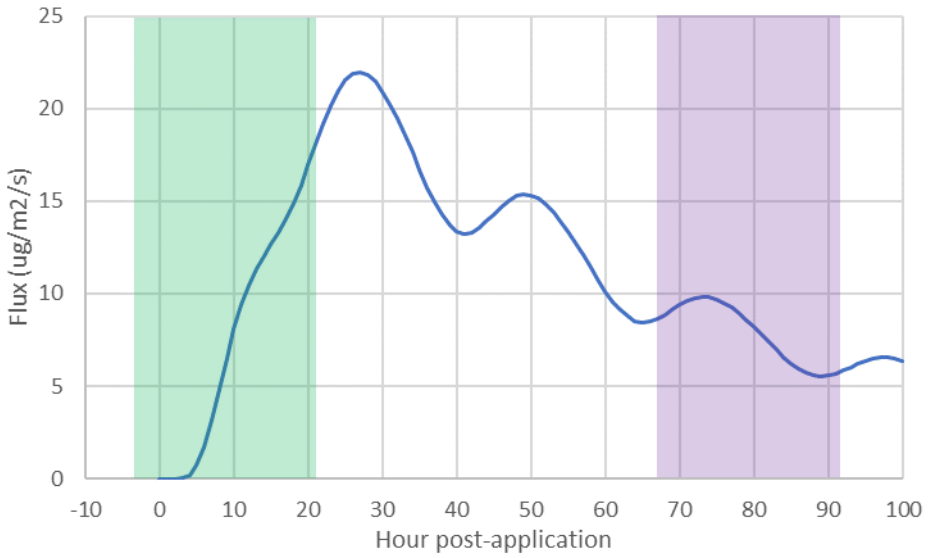


Figure 8. Relative timing between the 1,3-D applications and sampling periods, showing the 2022 flux profiles of FFM 1206 for soils #5 as an example. Highlighted are the sampling periods for hours -3~20 (green) and 68~91 (purple) aligned in the modeling for the high detections [5] (24.93, Parlier, 9/8/2021) and [3] (10.61 ppb, Parlier, 10/16/2020), respectively.

## 5.3 Spatial and temporal modeling on the high detections

The previous simulations (Figure 4 and Table 4) modeled the effects of the variations on the soil properties, and the results captured 4 of the 8 high detections of 1,3-D. Additional evaluations are conducted for the other 4 high detections ([2], [3], [7], and [8]) underestimated by the standard regional simulations. Additional evaluations consider the uncertainties on hourly emission fluxes and wind directions (section 4.3), and establish a probability distribution of predicted concentrations for each high detection. For each high detection, the additional evaluations include 925,000 model runs by considering 37 flux profiles (16 in the 2019 profiles and 21 in the 2022 profiles), 25 hours (±12 hours for shifting hourly fluxes, Figure 3), and 1,000 Monte Carlo simulations for wind directions. The standard regional simulation discussed in the previous section is actually one of the model runs without shifting on either hourly fluxes or wind direction (i.e., $dt = 0$ and $d\vartheta = 0$).

All high detections are well modeled with the additional evaluations (Table 6). Modeling results with uncertainties on flux profiles or wind direction only are also reported. By only considering the spatial uncertainty, the model captured most of the high detections, except for [8] (37.50 ppb, Shafter, 10/16/2020). The sole consideration of temporal uncertainty fails to model any high detections, but still improves the model performance compared to the standard regional modeling results (Table 4).

Table 6. Modeling results based on additional evaluations with uncertainties on hourly emission fluxes and wind directions

| ID | Site | Start date | Measured conc. (ppb) | Model performance by considering uncertainties in | | |
|---|---|---|---|---|---|---|
| | | | | Flux only | Wind direction only | Both |
| [2] | Parlier | 10/09/2018 | 111.29 | 58% | S | S |
| [3] | Parlier | 10/16/2020 | 10.61 | 96% | S | S |
| [7] | Shafter | 01/12/2020 | 20.80 | 21% | S | S |
| [8] | Shafter | 10/16/2020 | 37.50 | 49% | 76% | S |

Notes: "S" for satisfactory modeling (i.e., the measurement is captured by the predicted range). Otherwise, a P/O ratio is reported for underestimation. The percentages of variances are determined by a general linear model and normalized by the total variances explained by the 3 variables under evaluation. The other 4 high detections ([1], [4], [5], and [6]) have been well modeled by the standard regional simulations (Table 4) and thus do not need additional evaluations.

Results of general linear model on the model input and outputs indicate that majority (more than 80%) of the modeled variances on the predictions are attributed to the soils (modeled as various flux profiles) and wind directions. This is consistent with the previous efforts to improve the modeling performance on 1,3-D high detections with either receptor locations (Barry, 2015; Johnson, 2014; Luo, 2019a; van Wesenbeeck et al., 2013) or soil properties (Tao, 2018a, b, 2019).

## 6 Discussions and recommendations

Compared to regional, long-term regulatory modeling which mainly relies on reasonable estimates on the total and peak emissions, site-specific modeling for high detections requires accurate hourly flux data, hourly meteorological data, and their precise alignment during the sampling hours at the monitoring site location. In addition to the limitations of the Gaussian plume algorithm implemented in the AERMOD, the performance for site-specific modeling is related to the variabilities and uncertainties on the model input data.

Model predictions vary greatly with the flux profiles generated from different soil datasets (Figure 4 and Figure 5). For most of the modeled high detections, the maximum predictions were associated with the flux profile of soil #5, which represents the worst-case condition in the DPR-sampled soils prior to fumigation. However, there could be other extreme field conditions in reality associated with even higher emission of 1,3-D. For example, Tao (2019) evaluated a hypothetic condition for soil #5 with zero soil OC content, which would increase the predicted concentration by 15%.

Additional efforts on the emission fluxes are needed for better simulation of high detections. One proposed approach is to use site-specific inputs (rather than the template soil and weather data) to generate "onsite" flux profiles, while remain other HYDRUS model configurations and domain geometries. Except for soil water content, representative values for the soil properties, if not measured in the field during the sampling period, can be derived from soil database such as the Soil Survey Geographic Database (SSURGO). The soil water content can be statistically

sampled based on an empirical probability distribution or, if applicable, the information reported during soil preparation for fumigation. Finally, a series of flux profiles can be generated for the site-specific conditions and also represent the potential distribution of the soil water content.

Another consideration related to 1,3-D high detection modeling is the emission during soil fumigations, which is not represented in the flux profiles used in the current modeling. Results of field measurements and flux determination by DPR and DAS suggested that there could be high emission fluxes of 1,3-D during fumigations. Those high flux values would significantly contribute to the measured concentrations especially for the 1,3-D applications immediately before or after the start of sampling. For the high detection [7] (20.8 ppb, Shafter, 1/12/2020) as an example, the primary source is reported with an application time just 1 hour before the start of sampling. With the currently used flux profiles (e.g., Figure 8), therefore, there could be a potential underestimation of source emissions during the early hours of sampling period. Actually, most of the high detections are associated with this issue (Figure 10), including the high detection [1] (-6 hours), [2] (-7 hours), [4] (-6 hours), [5] (+3 hours), [7] (-1 hour), and [8] (-3 hours).

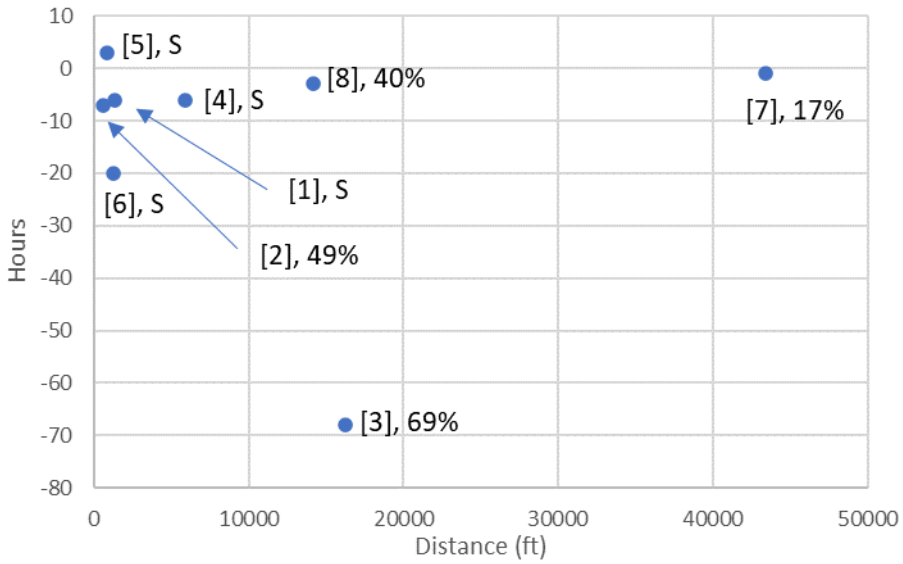


Figure 10. Modeling performance (standard regional simulations in Table 4) related to the estimated time intervals and distances between the sampling site/period and the primary sources. Negative hours for 1,3-D applications reported prior to the start of sampling.

The modeling performance generally declines with the increase of the distances between the monitoring site and the primary sources (Figure 10). For the 1,3-D high detections with large distances, uncertainties on the emission flux and wind direction should be considered. AERFUM uses AERMOD as the air dispersion simulation engine, which assumes a steady-state wind field over the domain of all sources and receptors. For a large modeling domain, this assumption would result in significant uncertainties on wind speed, wind direction, travel time of pollutants, and associated relative timing between the emission flux and sampling period. For regulatory modeling, AERMOD is recommended to use within 50 km of the sources (USEPA, 2017). For

site-specific modeling such as the replication of high detections, results of this study suggest additional uncertainty analysis on source emission and wind data for air dispersion modeling with a source-receptor distance over 10,000 ft (approximately 3 km or 2 mi).

**Acknowledgments**

The author acknowledges Colin Brown, Jing Tao, Jazmin Gonzalez, Aniela Burant, Maziar Kandelous, Minh Pham, and Randy Segawa for valuable discussions and critical reviews in the initialization and development of this study.

**References**

Ajwa, H. (2021). Monitoring of 1,3-dichloropropene emissions from deep-ripped, deep shank non-tarped broadcast shank applications with straight shank design (Study ID: 2020-DOW-01). Ajwa Analytical Laboratories, LLC, Gilroy, CA.

Barry, T. (2005). Estimation of methyl isothiocyanate air concentrations associated with priority case number 026-KER-05. California Department of Pesticide Regulation.

Barry, T. (2015). Evaluation of the Air Dispersion Modeling Tool SOFEA2. California Department of Pesticide Regulation, Sacramento, CA.

Barry, T. and E. Kwok (2016). Updated (no December applications allowed) simulation of cancer risks associated with different township cap scenarios of Merced County for 1,3-dichloropropene. California Department of Pesticide Regulation, Sacramento, CA.

Brown, C. (2015). Correlating Agricultural Use with Ambient Concentrations of the Fumigant Chloropicrin During the Period of 2011-2014, PDF. California Department of Pesticide Regulation.

Brown, C. (2016). Correlating agricultural use with ambient concentration of 1,3-Dichloropropene during the period of 2011-2014. California Department of Pesticide Regulation, Sacramento, CA.

Brown, C. (2019). HYDRUS-simulated flux estimates of 1,3-Dichlorpropene max period-averaged flux and emission ratio for approved application methods. California Department of Pesticide Regulation, Sacramento, CA.

Brown, C. (2022). Updates to HYDRUS-simulated flux estimates of 1,3-dichloropropene maximum period-averaged flux and emission ratios. California Department of Pesticide Regulation, Sacramento, CA.

Budahn, A. (2016). Correlating Agricultural Use with Ambient Air Concentrations of Chlorpyrifos and Chlorpyrifos-Oxon During the Period of 2011-2014, PDF. California Department of Pesticide Regulation.

CDPR (2015). 1,3-Dichloropropene Risk Characterization Document, Inhalation Exposure to Workers, Occupational and Residential Bystanders and the General Public. California Department of Pesticide Regulation, Sacramento, CA.

Collins, C. (2016). Correlating Agricultural Use with Ambient Air Concentrations of Methyl Isothiocyanate during the period of 2011-2014. California Department of Pesticide Regulation.

Craig, K. and A. Budahn (2016). Correlating Agricultural Use with Ambient Air Concentrations of Methyl Bromide During the Period of 2011- 2014. California Department of Pesticide Regulation.

DPR (2021). Risk management directive and mitigation guidance for acute, non-occupational bystander exposure from 1,3-Dichloropropene (1,3-D). California Department of Pesticide Regulatin.
Johnson, B. (2007a). Simulation of Concentrations and Exposure Associated with Dow Agrosciences-Proposed Township Caps for Merced County for 1,3-Dichloropropene. California Department of Pesticide Regulation, Sacramento, CA.
Johnson, B. (2007b). Simulation of concentrations and exposure associated with Dow AgroSciences-proposed township caps for Ventura County for 1,3-dichloropropene. California Department of Pesticide Regulation, Sacramento, CA.
Johnson, B. (2014). Comparison of one-year township monitoring results from Merced to SOFEA simulation results. California Department of Pesticide Regulation, Sacramento, CA.
Kandelous, M. and C. Brown (2019). Effect of pre-application soil moisture on emissions of 1,3-Dichloropropene. California Department of Pesticide Regulation, Sacramento, CA.
King, K. D. (2016). Correlating Agricultural Use with Ambient Air Concentrations of Chlorthal-Dimethyl During the Period of 2011-2014. California Department of Pesticide Regulation.
Luo, Y. (2017). Meteorological data processing for ISCST3 and AERMOD. California Department of Pesticide Regulation, Sacramento, CA.
Luo, Y. (2019a). Evaluating AERMOD for simulating ambient concentrations of 1,3-Dichloropropene. California Department of Pesticide Regulation, Sacramento, CA.
Luo, Y. (2019b). AERFUM: an integrated air dispersion modeling system for soil fumigants. California Department of Pesticide Regulation, Sacramento, CA.
Luo, Y. (2022). Modeling for the township cap of 1,3-Dichloropropene applications, modeling approach #2. California Department of Pesticide Regulation, Sacramento, CA.
Marks, T. (2016). Risk management directive and mitigation guidance for cancer risk from 1,3-Dichlorpropene (1,3-D). California Department of Pesticide Regulation, Sacramento, CA.
Miller, C. W. and L. M. Hively (1987). A review of validation studies for the Gaussian plume atmospheric dispersion model. Nuclear Safety 28(4): 522-531.
Rotondaro, A. and I. van Wesenbeeck (2012). Montoring of Cis-and Trans-1,3Dichlorpopropene in air in 9 high 1,3-Dichlorpopropene use townships Merced County, California. Regulatory Sciences and Government Affairs – Indianapolis Lab. DowAgroSciences LLC. 9330 Zionville Road, Indianapolis, Indiana 46268-1054. Data volume50046-0220 parts 1 and 2.
Sajo, E. (2003). An estimate of spatial uncertainty of mean concentrations predicted by Gaussian dispersion models. Health Phys 85(2): 174-183.
Segawa, R., P. Wofford and C. Ando (2006). Environmental justice pilot project protocol for pesticide air moniotoring in Parlier. California Department of Pesticide Regulation, Sacramento, CA.
Tao, J. (2016). Analysis of Agricultural Use and Average Concentrations of 1,3-Dichloropropene in Nine Communities of California in 2006 – 2015, and Calculation of a Use Limit (Township Cap). California Department of Pesticide Regulation, Sacramento, CA.
Tao, J. (2018a). Modeling a 1,3-Dichloropropene Application at Shafter, CA on January 21, 2018. California Department of Pesticide Regulation, Sacramento, CA.
Tao, J. (2018b). Modeling a 1,3-Dichloropropene Application at Parlier, CA on September 19, 2017. California Department of Pesticide Regulation, Sacramento, CA.

Tao, J. (2019). Modeling 1,3-Dichloropropene Applications at Parlier, CA on October 9, 2018. California Department of Pesticide Regulation, Sacramento, CA.

USEPA (2005). Revision to the guideline on air quality models: adoption of a preferred general purpose (flat and complex terrain) dispersion model and other revisions; final rule. 40 CFR Part 51. United States Environmental Protection Agency, Washington, DC.

USEPA (2017). 40 CFR Appendix W to Part 51, Guideline on Air Quality Models. United States Environmental Protection Agency, Washington, DC.

van Wesenbeeck, I. J., S. A. Cryer and O. de Cirugeda Helle (2013). Validation of SOFEA2 with 1,3-Dichloropropene ambient monitoring data in Merced County California – REVISED report [revised March 2014]. Regulatory Science and Governnment Affairs, Dow AgroSciences LLC 9330 Zionsville Road, Indianapolis, Indiana 46268-1054. Lab Study ID 131271.

Wilhoit, L., M. Zhang and L. Ross (2001). Data quality of California's Pesticide Use Report. Final Report to the California Department of Food and Agriculture for Contract Agreement NO. 980241. California Department of Pesticide Regulation.

Yamartino, R. J. (1984). A Comparison of Several "Single-Pass" Estimators of the Standard Deviation of Wind Direction. Journal of Applied Meteorology and Climatology 23(9): 1362-1366.

## Appendix I. Field fumigation methods (FFMs) for 1,3-D in California

Table 7. Field fumigation methods (FFMs) during the study period (2017-2021) for 1,3-D in California

| Method Name | Field Fumigation Method (FFM) Code |
|---|---|
| Nontarp/shallow/broadcast or bed | 1201 |
| Tarp/shallow/broadcast | 1202 |
| Tarpaulin/Shallow/Bed | 1203 |
| Nontarpaulin/Shallow/Broadcast or Bed/Three water treatment | 1204 |
| Tarpaulin/Shallow/Bed/Three Water Treatments | 1205 |
| Nontarp/18 inches deep/broadcast or bed | 1206 |
| Tarp/18 inches deep/broadcast | 1207 |
| Chemigation (drip system)/tarp | 1209 |
| Nontarp/18 inches deep/strip | 1210 |
| Nontarp/18 inches deep/GPS targeted | 1211 |
| Totally Impermeable Film (TIF) tarp/shallow/broadcast | 1242 |
| TIF tarp/shallow/bed | 1243 |
| TIF tarp/shallow/bed/3 water treatments | 1245 |
| TIF tarp/deep/broadcast | 1247 |
| TIF tarp/deep/strip | 1249 |
| Chemigation (drip)/ TIF tarp | 1259 |
| Other label method | 1290 |